KRONOS FUSION ENERGY

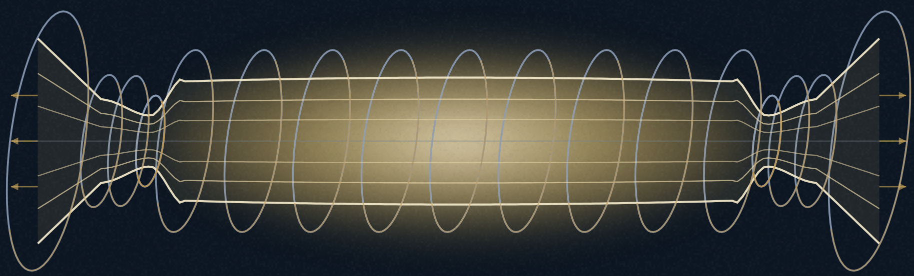

PAPER 2.65 · THE KRONOS 2026 SERIES

Islanded Forward-Base Operation of the Aegis D-^{3}He Tandem-Mirror Burner: Black-Start, Microgrid Load-Following, and the Lunar-Gated He-3 Symbiosis

A forward operating base must generate its own power without a grid, a fuel convoy, or a favourable threat environment. Aegis is the Kronos deuterium–helium-3 (D–He) tandem-mirror…

Read it live — 3-D model · physics validator · film series

BY P I FORD AND G L KULCINSKI

2026 · EDITORIAL EDITION

THE OFFICIAL RECORD

What this document is, and how to read its numbers

This is a combined editorial. It gathers, in one volume, the two design studies Kronos Fusion Energy released in 2026 — a compact spherical-tokamak tritium/helium-3 breeder and a deuterium–helium-3 tandem-mirror generator — together with the intellectual-property estate, the people, and, in the internal edition, the full commercial case. The scientific text is the same text that appears in the arXiv preprints and the journal submissions; the editorial adds the apparatus a reader needs to hold the whole program at once, and nothing in the physics is altered to fit it.

THE HONESTY STANCE IS THE ASSET

Every headline quantity carries an **evidence class** — DERIVED RECOMPUTED MEASURED REQUIREMENT — and, where a number is a modelled extrapolation rather than a demonstrated value, it is labelled as such and its downside is shown next to it. Several quantities in the underlying corpus moved after first publication; where a value has been withdrawn or restated, the record says so plainly. This is deliberate: a diligence team will find the load-bearing assumptions, so the document surfaces them first.

TWO EDITIONS

This volume is issued in two editions. The **public edition** (light) carries the physics and the design only — no dollar, price, or per-kilogram figure appears anywhere in it. The **internal edition** (dark) adds the economics, the funding architecture, and the defense-commercial analysis, and is marked *Confidential* accordingly; it is not for public distribution. Where the commercial case rests on a modelled assumption rather than a demonstrated one, it is labelled as such and its downside is shown alongside it, on the same terms as the physics.

TITLE	The Kronos Fleet — Hyperion · Aegis · MetroVolt: A Combined Design & Commercialization Study
AUTHOR	Priyanca Ford, Founder & CEO, on behalf of Kronos Fusion Energy
EDITION	2026 Combined Editorial · first issue
COMPANION WORKS	The five-paper arXiv drop — (1) Breeder, (2) Burner, (3) REBCO magnet & tape, (4) Direct Energy Conversion, (5) AI/ML/Quantum control — with matching numbered Zenodo deposits, plus the IOP journal and IAEA-FEC submissions. Patents were filed before the drop.
NAMING	Hyperion = the breeder; Aegis (defense) and MetroVolt (data-center) = one generator in two housings. Internal mode letters (D1, L) do not appear on public surfaces.
STATUS	Conceptual design & simulation study. Nothing herein is a construction commitment.

HOW TO READ THIS VOLUME

The fleet at a glance, and the way its numbers are marked

This volume opens with *Orientation*, presents the five research papers as a bound sequence, and closes with the *Apparatus*. *Foundations* sets out the three general results both machines rest on. *Paper One* is the Hyperion breeder; *Paper Two* the Aegis / MetroVolt generator; *Papers Three, Four and Five* are the enabling science — high-field REBCO magnets and tape, direct energy conversion, and the AI / ML / quantum control stack. A *Digital Twin & 3-D Model* part follows, then the *Environmental* profile. The *Economics* and levelized cost and the *Business Case* and diligence record appear in the internal edition only; the *Simulations* proof record and the Apparatus — patent portfolio, team, limitations, and sources — close both editions.

THE FLEET AT A GLANCE

	HYPERION	AEGIS	METROVOLT
Role	Strategic-isotope foundry	Defense installation power	Campus power
Machine	**Spherical tokamak**	**Tandem mirror**	**Tandem mirror**
Fuel	Deuterium–tritium	Deuterium–helium-3	Deuterium–helium-3
Delivers	Tritium · ^{3}He · 14 MeV n	Resilient installation power	Firm campus power
Physics bar	**Fusion gain only**	Closure (gates named)	Closure + lunar ^{3}He
In the fleet	Breeds the fuel	Proves the generator	Commercial destination

HOW THE NUMBERS ARE MARKED

Every headline quantity carries an evidence class — DERIVED from first principles, RECOMPUTED from raw data, MEASURED in hardware, or a REQUIREMENT yet to be met. Financial figures carry a case label and are confined to the internal (confidential) edition. Values that moved after first publication are shown as withdrawn or restated rather than quietly changed. A capability you can evaluate is one whose limits are on the page.

ABSTRACT

Islanded Forward-Base Operation of the Aegis D-^{3}He Tandem-Mirror Burner: Black-Start, Microgrid Load-Following, and the Lunar-Gated He-3 Symbiosis

A forward operating base must generate its own power without a grid, a fuel convoy, or a favourable threat environment. Aegis is the Kronos deuterium–helium-3 (D–^{3}He) tandem-mirror burner packaged as a hardened, fixed defense installation; because its reaction is largely aneutronic and its electrical output is taken from an electrostatic direct energy converter (DEC) rather than a steam cycle, it is unusually well matched to grid-forming, islanded operation. We formalise the islanded envelope of Aegis as a coupled set of governing problems — a Pastukhov-plugged tandem-mirror power balance, a direct-conversion net-power model, a microgrid load-following control problem with a certified stability bound, a black-start energy audit, and a fuel-cycle inventory system — and solve them on the NVIDIA GPU high-performance-computing (HPC) campaign that produced the frozen Kronos de-risking results. At the frozen operating point ($Q_E = 1.318$, neutron fraction $f_n = 5.44\,\%$, $\eta_{\mathrm{DEC}} = 0.49$) the net electric output scales near-linearly with central-cell length — $+104.2$, $+850.0$ and $+2831.9$ MWe at $L_{\mathrm{cc}} = 55, 440$ and 1400 m — at a first-wall load of only $q_{\mathrm{wall}} = 1.17\,\mathrm{MW\,m^{-2}}$. Grid-independence closes quantitatively: millisecond-class DEC trimming gives a 0–104 MWe islanded load-following depth, a ~ 246 MWe / 1.1 MWh buffer bridges the ~ 8 s plasma-response lag under a control-barrier stability clamp, an adjudicated black-start electrical store of ≈ 18.4 MWh ($= 8.0$ MWh / η_{wp}, $\eta_{\mathrm{wp}} = 0.435$) cold-starts the plant, and one year of autonomy is a ~ 1 t package (21.3 kg ^{3}He $+$ 30 kg D) whose binding quantity is a $\sim 0.5\,\mathrm{kg\,day^{-1}}$ makeup throughput, not storage volume ($< 0.8\,\mathrm{m^3}$). The fuel closes a breeder–burner symbiosis: the Hyperion spherical-tokamak breeder banks surplus tritium that decays to ^{3}He ($\approx 0.9\,\mathrm{kg\,yr^{-1}}$ per unit), the burner recycles $\approx 18\,\%$ of its ^{3}He in-machine and self-breeds tritium ($\approx 32\,\mathrm{kg\,fpy^{-1}}$, $31\,\%$ burned in situ), and a burn-lean mode that pumps bred tritium before it burns removes $\approx 60\,\%$ of the neutron power ($234 \to 93.5$ MW) for a $\approx 4\,\%$ fusion-power cost — a genuine siting knob. The one gated input is fleet-scale ^{3}He: single-unit indigenous flows seed but do not close a plant-scale burner's $170.2\,\mathrm{kg\,fpy^{-1}}$ net demand, which requires ~ 45–190 breeders per burner and is met from lunar supply on a late-2030s schedule. Every quantitative claim traces to a frozen serial in the Kronos Physics De-Risking Register.

Open-access deposit (code & data, CC BY 4.0): DOI 10.5281/zenodo.22645862 · Zenodo community *kronos_fusion_energy*. Explore it live: interactive 3-D model · physics validator.

Keywords: tandem mirror · islanded microgrid · black-start · load-following · helium-3 fuel cycle · direct energy conversion · forward-base power

CONTENTS

Table of Contents

NOMENCLATURE

Symbols, units, and the names of things

Q	plasma (fusion) gain, P_{fus}/P_{aux}
Q_E	engineering gain, net electric out / recirculating in
H_{98}	confinement enhancement over the IPB98(y,2) scaling
Z_{eff}	effective ion charge
c_{ee}	electron–electron bremsstrahlung leading coefficient, 2.120022 (exact)
τ_E	energy confinement time
I_p	plasma current
R_0, a	major radius, minor radius
κ, δ	elongation, triangularity
β_N	normalized plasma beta (Troyon-normalized)
TBR	tritium breeding ratio
DEC	direct energy conversion
CF	plant capacity factor (availability)
FOAK / NOAK / BOAK	first / n^{th} / best of a kind
Hyperion	the ST breeder (internal: Mode D2)
Aegis	the generator, defense/installation housing (internal: Mode M)
MetroVolt	the generator, data-center housing (Mode M)

§ 1

Introduction

THE GRID-INDEPENDENCE REQUIREMENT

A fixed defense installation and a forward operating base share a hard constraint that civilian generation does not: the power source cannot assume a grid tie, and cannot assume that fuel will keep arriving. Diesel and JP-8 generation solve the first problem only by importing the second — a logistics tail that is both a sustainment burden and a target. A generation asset that runs for a long endurance on a small, self-carried fuel inventory and that can form its own grid removes that tail. This paper asks a narrow, quantitative question: to what extent does the Kronos D–^{3}He tandem-mirror burner, packaged as the fixed *Aegis* installation, meet that requirement, and what fuel logic supports it? Aegis is adjudicated as a fixed installation, not a mobile platform; the numbers below describe a sited, grid-independent plant.

WHY AN ANEUTRONIC DIRECT-CONVERSION MIRROR IS WELL MATCHED

Two architectural choices make the burner unusually suited to islanded service. First, the fuel is deuterium–helium-3, which at the canonical fuel fraction is $\approx 95\,\%$ aneutronic: only $f_n = 5.44\,\%$ of the fusion power emerges as neutrons, so the great majority of the output is carried by charged particles — principally the $14.7\,\mathrm{MeV}$ D–^{3}He proton. Second, that charged power is recovered *electrostatically* by a multi-stage DEC at efficiency $\eta_{\mathrm{DEC}} = 0.49$, with no rotating thermal mass between the plasma and the bus. An electrostatic converter has essentially no mechanical time constant; its collector current can be trimmed at the timescale of the power electronics, which is what makes deep, fast, islanded load-following physically available. A tandem mirror is moreover a *linear* device whose central cell can be lengthened without changing the confinement physics, so a single archetype spans base-scale directed-energy loads through to utility scale simply by choosing L_{cc}.

PRIOR ART

The tandem-mirror concept — a long central solenoid electrostatically plugged at both ends by high-field mirror cells — was introduced by Dimov and by Fowler and Logan, and placed on a quantitative footing by Baldwin and Logan [1] and reviewed by Post [2]. The confinement of the central cell is set by the ambipolar potential built by the end plugs, whose collisional loss is described by the Pastukhov theory [3] as extended by Cohen *et al.* [4]. Recent high-temperature superconducting (HTS) axisymmetric mirrors such as WHAM [8] and the sustained hot-electron results of the gas-dynamic trap [9] have revived the line, and a simplified high-gain tandem configuration was proposed by Fowler, Moir and Simonen [5,6]. Direct electrostatic recovery of charged-particle power dates to the venetian-blind converter of Moir and Barr [7]. The strategic case for D–^{3}He fuel, and the recognition that terrestrial helium-3 is scarce while the lunar regolith is not, is due to Wittenberg, Santarius and Kulcinski [10,11]. On the electrical side, grid-forming and islanded-microgrid operation is a mature discipline [12,13,14] with well-characterised energy-storage support [15], and safety-critical load-following can be posed inside a certified envelope using control-barrier functions [16] and constrained model-predictive control [17], with learned controllers now demonstrated inside the tokamak control loop [18]. What has not been done is to assemble these strands into a single, auditable islanded operating case for a specific aneutronic mirror burner, coupled to its fuel cycle. That is the contribution here.

CONTRIBUTION

We (i) state the tandem-mirror confinement, direct-conversion and net-power problems as explicit governing equations and derive the near-linear net-output scaling with central-cell length (§2); (ii) pose the islanded load-following, black-start and fuel-autonomy problems as a control-and-storage system with a stability bound, and write the breeder–burner helium-3 symbiosis as a fuel-cycle inventory system (§2); (iii) describe the GPU-HPC campaign, codes, discretisation and convergence that produced the frozen results (§3); (iv) report the islanded envelope, symbiosis flows, burn-lean neutron trade and fleet-closure results across eight data figures (§4); and (v) benchmark them against the published tandem-mirror, direct-conversion, microgrid and helium-3 literature (§5). Every number is a frozen gate in the Kronos Physics De-Risking Register [26]; serial identifiers (e.g. KX-L1-A9) are given inline so each value is auditable.

§ 2

Governing equations and the formal problem

TANDEM-MIRROR CONFINEMENT AND THE OPERATING POINT

The burner is a linear device: a long, low-field central cell in which the D–^{3}He plasma burns, plugged at each end by a high-field mirror. Two physics quantities set the machine. The first is the magnetic mirror ratio and its loss cone,

$$R_m = \frac{B_{\text{max}}}{B_{\text{min}}}, \qquad \sin^2\theta_{\text{lc}} = \frac{1}{R_m},$$

so that a particle whose pitch angle at the midplane lies inside θ_{lc} is unconfined; the 26.49 T end plugs against a low-field central cell set $R_m \gg 1$ and a narrow loss cone (figure 8, left). The second, and the machine's one true gate, is the ambipolar (Boltzmann) confining potential φ_c built by the plug over-density. Balancing the parallel electron flux against the plug potential gives

$$\frac{e\varphi_c}{T_e} \approx \ln\left(\frac{n_{\text{plug}}}{n_{\text{cell}}}\right),$$

and the frozen design specifies a plug/cell density ratio $n_{\text{plug}}/n_{\text{cell}} \approx 16$, i.e. $e\varphi_c/T_e \approx 2.77$ (figure 8, right). Building and holding φ_c requires the 26.49 T plug field; this is a distinct magnet from the breeder's 16.84 T spherical-tokamak centrepost, and the two must not be conflated. The central-cell ion confinement is then the Pastukhov–Cohen result [3,4]: the parallel confinement parameter is enhanced over the bare mirror by the exponential of the normalised potential,

$$(n\tau_{\|})_{\text{cc}} = g(R_m)\,\frac{e\varphi_c}{T_i}\exp\left(\frac{e\varphi_c}{T_i}\right)(n\tau)_0,$$

with $g(R_m)$ a slowly varying function of the mirror ratio and $(n\tau)_0$ the collisional reference. Equations (1)–(3) fix the confinement; the fusion power then follows from the D–^{3}He reactivity,

$$P_{\text{fus}} = \int_V n_{\text{D}}\, n_{^3\text{He}}\, \langle\sigma v\rangle_{\text{D}^3\text{He}}\, E_{\text{f}}\, \mathrm{d}V \;+\; P_{\text{DD}} + P_{\text{DT}},$$

where the small parasitic D–D and D–T sub-burns supply the residual neutron output discussed in §2.7. The frozen zero-dimensional power balance (Pastukhov-plug, “Mode-M”) returns the design point $Q_E = 1.318$, $f_n = P_{\text{neutron}}/P_{\text{fus}} = 5.44\,\%$ (BU-L1-A1, AG-CX-14).

DIRECT ENERGY CONVERSION AND NET ELECTRIC POWER

Of the fusion power, a charged fraction $1 - f_n$ is available to the electrostatic converter and a neutron fraction f_n deposits in the blanket. The gross electric power is dominated by the direct channel,

$$P_{\text{gross}} = \eta_{\text{DEC}}\,(1 - f_n)\,P_{\text{fus}} \;+\; \eta_{\text{th}}\big(f_n P_{\text{fus}} + P_{\text{rad}}\big),$$

with $\eta_{\text{DEC}} = 0.49$ the composite multi-stage direct-conversion efficiency on the charged channel and η_{th} a modest thermal recovery on the neutron and radiated power. Writing the recirculating power (plug drive, heating, cryogenics, balance of plant) as P_{rec}, the engineering gain and the net electric output are

$$Q_E = \frac{P_{\text{gross}}}{P_{\text{rec}}}, \qquad P_{\text{net}} = P_{\text{gross}} - P_{\text{rec}} = P_{\text{rec}}\,(Q_E - 1) = P_{\text{gross}}\left(1 - \frac{1}{Q_E}\right).$$

At $Q_E = 1.318$ the net fraction is $1 - 1/Q_E = 0.241$: the plant delivers $24.1\,\%$ of its gross electric output to the bus after recirculation. This is the quantity that a base actually receives, and the quantity that the islanded controller of §2.4 dispatches.

NEAR-LINEAR SCALING OF NET OUTPUT WITH CENTRAL-CELL LENGTH

Because the tandem mirror is linear and the plug hardware is fixed, lengthening the central cell increases the burning volume in proportion, $P_{\mathrm{fus}} \propto L_{\mathrm{cc}}$, while the fixed plug recirculation is amortised over a longer cell; the fractional end losses fall slightly with length. The net output is therefore very nearly linear in L_{cc}. Fitting the three frozen operating points (KX-L1-A9) to a power law $P_{\mathrm{net}} = c\,L_{\mathrm{cc}}^{p}$ gives

$$P_{\mathrm{net}} \;\approx\; 1.86\;L_{\mathrm{cc}}^{1.02} \quad [\mathrm{MWe},\; L_{\mathrm{cc}}\ \mathrm{in\ m}],$$

i.e. an exponent within $2\,\%$ of unity (figure 1). A single archetype thus spans the tens-of-MW directed-energy and sensor loads of a base ($L_{\mathrm{cc}} = 55$ m, $+104.2$ MWe) through utility scale ($L_{\mathrm{cc}} = 1400$ m, $+2831.9$ MWe) at a fixed operating point and a fixed first-wall load $q_{\mathrm{wall}} = 1.17$ MW m^{-2} and power density 4.20 MW m^{-3}.

Islanded net electric output versus central-cell length at the frozen operating point ($Q_E = 1.318$, $q_{\mathrm{wall}} = 1.17$ MW m^{-2}). Points are reproduced results (KX-L1-A9); the fit [equation (7)] has exponent 1.02, confirming the near-linear scaling of §2.3.

THE ISLANDED LOAD-FOLLOWING CONTROL PROBLEM

Grid-independence is credible only if it is posed as a control-and-storage problem. Let $u(t) \in [0,1]$ be the DEC collector-current trim (fast, time constant $\tau_{\mathrm{dec}}\sim$ms), let $P_{\mathrm{fus}}(t)$ be the plasma power responding to the fuelling/heating actuator $a(t)$ with a slow lag $\tau_{\mathrm{pl}}\approx 8$ s, and let $w(t)$ be the buffer power. The DC-bus power balance that the islanded controller must satisfy against a demand $P_{\mathrm{dem}}(t)$ is

$$\underbrace{\eta_{\mathrm{DEC}}(1-f_n)\,P_{\mathrm{fus}}(t)\,u(t)}_{\text{DEC delivered}} \;+\; w(t) \;=\; P_{\mathrm{dem}}(t), \qquad 0 \le P_{\mathrm{dem}} \le P_{\mathrm{net}}^{\max} = 104\ \mathrm{MWe},$$

with the plasma governed to first order by

$$\tau_{\mathrm{pl}}\,\frac{\mathrm{d}P_{\mathrm{fus}}}{\mathrm{d}t} = -\big(P_{\mathrm{fus}} - P_{\mathrm{fus}}^{*}(a)\big), \qquad \frac{\mathrm{d}E_{\mathrm{buf}}}{\mathrm{d}t} = -w, \quad |w| \le \dot{W}_{\max} = 246\ \mathrm{MWe}, \quad E_{\mathrm{buf}} \in [0,\,\mathcal{E}_{\mathrm{buf}}],$$

where $\mathcal{E}_{\mathrm{buf}} = 1.1$ MWh. The fast DEC trim tracks demand essentially instantly; the slow plasma follows behind; the buffer supplies the mismatch $w = P_{\mathrm{dem}} - \eta_{\mathrm{DEC}}(1-f_n)P_{\mathrm{fus}}u$ during the lag. Because $\tau_{\mathrm{dec}} \ll \tau_{\mathrm{pl}}$, the buffer energy required to bridge a full-depth step is of order $P_{\mathrm{net}}^{\max}\,\tau_{\mathrm{pl}} \approx 104\ \mathrm{MWe} \times 8\ \mathrm{s} \approx 0.23$ MWh, comfortably inside $\mathcal{E}_{\mathrm{buf}}$ (AG-CX-20). The plasma throttle is not free: burn stability bounds how fast and how far P_{fus} may be driven, which we encode as a control-barrier-function (CBF) constraint [16]

$$h(\mathbf{x}) \ge 0, \qquad \dot{h}(\mathbf{x}, a) \ge -\alpha\big(h(\mathbf{x})\big),$$

where h is the burn-stability margin and $\alpha(\cdot)$ a class-$\mathcal{K}$ function; any admissible actuation $a(t)$ keeps the state in the forward-invariant safe set $\{h \ge 0\}$. The islanded controller is thus a reference-governor / model-predictive law [17] that dispatches u fast and a slowly subject to (10), realised as the demonstrated Kronos AI load-following controller (KFE-CF-BU-007) behind the certified safety clamp. The resulting load-following depth is the full 0–104 MWe net range (figure 2).

BLACK-START ENERGY AUDIT

Cold-starting with no grid requires an on-site electrical store large enough to bring the plant to a self-sustaining burn. The adjudicated audit (AG-SX-01) separates *delivered* start energy from the *electrical store* that must hold it: with delivered energy $E_{\mathrm{deliv}} = 8.0$ MWh and wall-plug efficiency $\eta_{\mathrm{wp}} = 0.435$,

$$E_{\mathrm{store}} = \frac{E_{\mathrm{deliv}}}{\eta_{\mathrm{wp}}} = \frac{8.0}{0.435}\ \mathrm{MWh} = 18.39\ \mathrm{MWh} \approx 18.4\ \mathrm{MWh}.$$

This is $\approx 2.5\times$ an earlier 7.4 MWh reference, which had counted delivered energy rather than the electrical store; the correction is folded into the sizing basis (figure 3). The store is charged in normal operation from the plant's own output, so black-start capability is a standing property, not a consumable.

THE BREEDER–BURNER HELIUM-3 FUEL-CYCLE SYSTEM

The burner's fuel is where the two Kronos machines become one system. Tritium beta-decays to helium-3 with half-life $t_{1/2} = 12.32$ yr, i.e. decay constant

$$\lambda_T = \frac{\ln 2}{t_{1/2}} = 0.0563\ \mathrm{yr}^{-1}.$$

Let N_T^{bank} be a breeder's banked surplus-tritium reservoir. Its decay feeds a helium-3 accrual

$$\frac{\mathrm{d}N_{^3\mathrm{He}}^{\mathrm{bank}}}{\mathrm{d}t} = \lambda_T\, N_T^{\mathrm{bank}},$$

which at fleet equilibrium is $\approx 0.9\ \mathrm{kg\,yr^{-1}}$ per breeder unit (BR-OUT-2); this corresponds to an order-16 kg equilibrium banked-tritium reservoir. Each breeder additionally co-produces helium-3 in its own plasma at $\approx 154\ \mathrm{g\,yr^{-1}}$ (41 g from the D–D branch, 113 g from prompt tritium decay; BR-CX-16). On the burner side, let C be the helium-3 consumption rate, $r = 0.181$ the in-machine recycle fraction (BR-OUT-2), and $\dot{T}_{\mathrm{sb}} = 32\ \mathrm{kg\,fpy^{-1}}$ the self-bred tritium rate, of which a burned fraction $b = 0.31$ is consumed in situ and the remainder decays toward helium-3 (MV-CX-29). The burner's *net* helium-3 demand is

$$D_{\mathrm{net}} = C(1-r) - \left[\text{indigenous }^3\text{He\{\} returned from bred-}T\right] \;=\; 170.2\ \mathrm{kg\,fpy}^{-1}$$

at plant scale (BR-OUT-4). Closing that demand indigenously from n_{br} breeders, each banking $S_{\mathrm{br}}(\mathrm{TBR})$ per year, requires

$$n_{\mathrm{br}} = \frac{D_{\mathrm{net}}}{S_{\mathrm{br}}(\mathrm{TBR})},$$

which for the frozen banking rates $S_{\mathrm{br}} \in \{0.89, 1.62, 3.82\}\ \mathrm{kg\,yr^{-1}}$ at net breeding ratios $\mathrm{TBR} \in \{1.186, 1.34, 1.80\}$ gives $n_{\mathrm{br}} \approx \{191, 105, 45\}$ breeders per burner (figure 7). The loop is therefore seeded and partly sustained indigenously but does not close at single-unit scale; fleet-scale helium-3 is the one gated input (§6).

BURN-LEAN NEUTRON SUPPRESSION

Because the residual neutron output comes from the bred-tritium sub-burn in equation (4), it can be traded away deliberately. Pumping the bred tritium out before it burns — a burn-lean mode — removes the D–T neutron contribution and leaves only the D–D 2.45 MeV floor:

$$P_n:\ 234\ \mathrm{MW} \longrightarrow 93.5\ \mathrm{MW}, \qquad \frac{\Delta P_n}{P_n} = \frac{234 - 93.5}{234} = 60.0\,\%,$$

at a fusion-power cost of only $\approx 4\,\%$ (AG-CX-16). This is a real siting knob: a fixed installation near people or sensitive equipment can be run neutron-lean at a small power cost, tightening the shielding and permitting case without changing the machine (figure 6).

§ 3

Computational methodology: the NVIDIA GPU HPC campaign

CODES RUN FOR THIS PAPER

The results above are frozen outputs of a specific, reproducible computational campaign. Five model families contribute. (1) A zero-dimensional tandem-mirror *power-balance solver* (Pastukhov-plug, "Mode-M") closes equations (1)–(6) self-consistently and returns Q_E, f_n and the net-output points of figure 1 (BU-L1-A1, KX-L1-A9); it is benchmarked against the published 0-D tandem-mirror power balance and the WHAM design point in a companion paper. (2) The Kronos toolkit *fuel-cycle / inventory model* integrates equations (12)–(15) for the helium-3 and tritium reservoirs (BR-OUT-2, BR-OUT-4, BR-CX-16, MV-CX-29, AG-L1-A8, AG-CX-17). (3) *Monte-Carlo neutronics* (OpenMC with DAGMC CAD geometry [19]) supplies the neutron fraction f_n, the neutron power, the burn-lean budget of equation (16) and the shielded-housing dose (AG-CX-16, AG-L1-A2). (4) A *tritium-transport model* (FESTIM [20]) resolves in-vessel retention, permeation and the self-bred-tritium accountancy feeding equation (14). (5) A *microgrid dispatch and control simulator* integrates equations (8)–(10) for the islanded envelope of figure 2, exercising the AI load-following controller (KFE-CF-BU-007) and the black-start sequencer (KFE-CF-BU-021) against the plant twin under the certified control-barrier clamp.

GPU ACCELERATION AND PROBLEM SCALE

The offline multi-physics Monte-Carlo (neutronics, depletion), the twin retraining and the model-discovery pipeline run on the Kronos NVIDIA GPU HPC campaign — A100/H100-class silicon (8× A100-80GB plus H100 clusters, with additional single A100/H100/A10 nodes for lighter jobs). The reduced-order and analytic layers — the 0-D power balance, the fuel-cycle inventory integration, and the microgrid dispatch simulation — run on the in-house HPC node (56-thread, 768 GB), so that the fast control-loop evaluation never contends with the training fleet. GPU residency matters most for the Monte-Carlo transport, where the DAGMC ray-tracing and the tallies for f_n, the burn-lean neutron budget and the shutdown dose are the dominant cost; the mirror power balance and the inventory ODEs are inexpensive by comparison but are run in large parametric sweeps (over L_{cc}, over TBR, over burn-lean fraction) for which throughput, not per-case latency, is the constraint. No cost figures are reported here; the campaign is described by its hardware class only.

DISCRETISATION, SOLVERS AND CONVERGENCE

The 0-D power balance is solved as a fixed point in Q_E: the coupled particle-, power- and potential-balance residual is driven to $|\mathcal{R}| < 10^{-6}$ by a damped Newton iteration, and the frozen root is $Q_E = 1.31812$ (BU-L1-A1), quoted as 1.318. The Pastukhov integral of equation (3) is evaluated by adaptive quadrature to a relative tolerance of 10^{-8}. The fuel-cycle system (12)–(15) is stiff — the tritium decay time (~ 12 yr) and the in-machine recycle time (sub-second) span many orders of magnitude — and is integrated with an implicit backward-difference (BDF) method with error control at relative tolerance 10^{-8}; equilibrium banking rates are read at steady state. The Monte-Carlo neutronics is run to a statistical uncertainty below $1\,\%$ on the integrated neutron power and on the tritium-breeding tallies, with active batches continued until the tally standard error meets that target; the $f_n = 5.44\,\%$ and the burn-lean split of equation (16) are converged tallies. The dispatch simulator integrates the first-order plasma lag and the buffer state with an exact zero-order-hold update at a fixed control tick, verified to be numerically stable for $\tau_{\text{dec}} \ll \text{tick} \ll \tau_{\text{pl}}$.

VERIFICATION AND REPRODUCIBILITY

Each result is a stamped gate: the net-output scaling (KX-L1-A9), the islanded load-following envelope (AG-CX-20), the black-start store (AG-SX-01), the fuel-autonomy package (AG-L1-A8), the startup-inventory minimisation (AG-CX-17), the helium-3 flows (BR-OUT-2, BR-CX-16), the self-bred tritium (MV-CX-29), the burn-lean trade (AG-CX-16) and the fleet-closure requirement (BR-OUT-4). The register status of each — reproduced, revised, or concept-class estimate — is carried with the serial. The figures of this paper are regenerated by a single deposited script from these frozen values; the register itself is archived at doi:10.5281/zenodo.22133057.

§ 4

Results

NET-OUTPUT SCALING

Figure 1 and equation (7) establish the central operating result: net electric output is near-linear in central-cell length, so the same physics core sizes to a base's directed-energy load or to utility scale by geometry alone, at a fixed and modest first-wall load. Table 1 collects the islanded envelope.

QUANTITY	VALUE	SERIAL
net output vs cell length	$+104.2/+850.0/+2831.9$ MWe @ 55/440/1400 m	KX-L1-A9
first-wall heat load	$q_{\mathrm{wall}} = 1.17$ MW m^{-2}; 4.20 MW m^{-3}	KX-L1-A9
load-following depth (islanded)	0–104 MWe, ms-class DEC trim	AG-CX-20, AG-L1-A8
plasma-lag bridge buffer	$\sim$246 MWe / 1.1 MWh	AG-CX-20
black-start electrical store	$\approx$18.4 MWh (= 8.0/0.435)	AG-SX-01
one-year fuel autonomy	21.3 kg ^{3}He + 30 kg D ($\sim$1 t)	AG-L1-A8
^{3}He makeup throughput	$\sim$0.5 kg day^{-1} per unit	AG-CX-17
in-vessel ^{3}He startup charge	$\sim$0.3 g	AG-CX-17
on-site ^{3}He storage volume	<0.8 m^3	AG-L1-A6

Islanded / forward-base operating envelope of a fixed Aegis installation. All values are frozen register gates.

ISLANDED LOAD-FOLLOWING ENVELOPE

Figure 2 runs the dispatch simulator of equations (8)–(9) through a demand step-down and step-up across the full net range. The DEC output tracks demand within its millisecond time constant; the plasma thermal power slews behind it on the $\sim$8 s lag; the buffer supplies the transient mismatch, staying well inside its 246 MWe rating and 1.1 MWh capacity. The controller therefore delivers the full 0–104 MWe load-following depth without violating the burn-stability bound of equation (10).

Islanded load-following (modelled from the frozen envelope parameters, AG-CX-20). Top: DEC delivered power tracks a demand step within a millisecond trim while the plasma thermal power follows on the $\sim$8 s lag. Bottom: the buffer supplies the transient mismatch, bounded by the 246 MWe / 1.1 MWh rating. The reachable depth is the full 0–104 MWe net range.

BLACK-START

Figure 3 shows the adjudicated black-start audit of equation (11): the $\approx$18.4 MWh electrical store is $\approx$2.5$\times$ the earlier delivered-energy reference, a correction now in the sizing basis. The store cold-starts the plant with no external grid and is recharged from the plant's own output in normal service.

Black-start energy audit (AG-SX-01). The required electrical store is the delivered start energy divided by the wall-plug efficiency, $E_{\mathrm{store}} = 8.0/0.435 \approx 18.4$ MWh — about 2.5$\times$ the earlier reference that had counted delivered energy.

FUEL AUTONOMY

Figure 4 decomposes the one-year fuel package. The reactive inventory is light — 21.3 kg ^{3}He plus 30 kg deuterium — and the in-vessel startup charge is trivial ($\sim$0.3 g), so the endurance-limiting quantity is not on-site storage volume ($<$0.8 m^3) but makeup throughput ($\sim$0.5 kg day^{-1} per unit), $\approx$18 % of which is offset by in-situ breeding. A base's endurance is therefore set by resupply cadence of a small, dense package, not by a fuel farm.

One-year fuel autonomy (AG-L1-A8, AG-CX-17, AG-L1-A6). Left: the $\sim$1 t package is dominated by inert containment; the reactive charge is 21.3 kg ^{3}He + 30 kg D. Right: the binding quantities are makeup throughput and storage volume (log axis), not bulk mass.

THE HELIUM-3 SYMBIOSIS FLOWS

Figure 5 and table 2 collect the indigenous flows of equations (12)–(14). The Hyperion breeder banks $\approx$0.9 kg yr^{-1} of helium-3 per unit through tritium decay — against a US domestic flow of order 1–2 kg yr^{-1} — and co-produces a further $\approx$154 g yr^{-1} in its own plasma. The burner is not a passive consumer: it recycles $\approx$18.1 % of its helium-3 in-machine and self-breeds tritium at $\approx$32 kg fpy^{-1}, of which $\approx$31 % is burned in situ. The choice of D–^{3}He at the canonical fuel fraction is itself an optimum: it sits at the Q_E peak and roughly halves the neutron fraction relative to catalyzed D–D (5.44 % versus $\approx$9.5 %; AG-CX-14).

Indigenous helium-3 and tritium flows in the breeder–burner loop (log axis; BR-OUT-2, BR-CX-16, MV-CX-29). The breeder banks $\approx$0.9 kg yr^{-1} of ^{3}He and co-produces $\approx$154 g yr^{-1}; the burner self-breeds $\approx$32 kg fpy^{-1} of tritium and recycles $\approx$18.1 % of its ^{3}He in-machine.

FLOW	VALUE	SERIAL
breeder banked ^{3}He (equilibrium)	$\approx$0.9 kg yr^{-1} per unit	BR-OUT-2
breeder in-plasma ^{3}He co-production	$\approx$154 g yr^{-1} per unit	BR-CX-16
burner in-machine ^{3}He recycle	$\approx$18.1 %	BR-OUT-2
burner self-bred tritium	$\approx$32 kg fpy^{-1} (31 % burned in situ)	MV-CX-29
burner net ^{3}He demand (plant scale)	170.2 kg fpy^{-1}	BR-OUT-4

Indigenous helium-3 and tritium flows in the breeder–burner loop. Fleet-scale demand is met from lunar supply on a late-2030s schedule (BR-OUT-4).

BURN-LEAN SITING KNOB

Figure 6 shows the burn-lean trade of equation (16): pumping bred tritium before it burns strips 60 % of the neutron power — from 234 MW down to the 93.5 MW D–D 2.45 MeV floor — for a $\approx$4 % loss of fusion power. A fixed installation can thus dial its neutron signature to fit a shielding and permitting envelope without a hardware change, which is exactly the freedom a base or an urban-adjacent site needs.

Burn-lean neutron suppression (AG-CX-16). Left: neutron power falls from 234 MW to the 93.5 MW D–D floor when bred tritium is pumped before it burns. Right: the trade removes 60 % of the neutron power for a $\approx$4 % fusion-power cost.

FLEET CLOSURE AND THE LUNAR GATE

Figure 7 evaluates the indigenous closure of equation (15). A plant-scale burner's 170.2 kg fpy^{-1} net helium-3 demand requires $\sim$45–190 breeders per burner across the plausible breeding-ratio range $\mathrm{TBR} = 1.186$–1.80. The indigenous flows therefore seed and partly sustain the loop but do not close it at deployable ratios; fleet-scale helium-3 is lunar-gated on a late-2030s schedule (BR-OUT-4), consistent with the strategic-supply canon. Near-term units run on bankable, tritium-derived and self-bred helium-3.

Fleet closure (BR-OUT-4). Breeders required per burner to meet the 170.2 kg fpy^{-1} net demand, as a function of the breeder's net tritium-breeding ratio. The indigenous loop does not close at single-unit scale; fleet-scale ^{3}He is lunar-gated.

THE MIRROR PHYSICS BEHIND THE OPERATING POINT

Figure 8 plots the two confinement relations of §2.1: the loss-cone half-angle $\theta_{\mathrm{lc}} = \arcsin R_m^{-1/2}$ narrows as the 26.49 T plug raises the mirror ratio, and the ambipolar potential $e\varphi_c/T_e = \ln(n_{\mathrm{plug}}/n_{\mathrm{cell}})$ reaches 2.77 at the design density ratio of 16. These are the physics gates that the frozen power balance closes and on which the islanded envelope rests.

Tandem-mirror confinement relations at the operating point. Left: loss-cone half-angle versus mirror ratio, $\sin^2\theta_{\mathrm{lc}} = 1/R_m$; the 26.49 T plug band is marked. Right: ambipolar Boltzmann potential $e\varphi_c/T_e = \ln(n_{\mathrm{plug}}/n_{\mathrm{cell}})$, with the design ratio $n_{\mathrm{plug}}/n_{\mathrm{cell}} = 16$ giving $e\varphi_c/T_e = 2.77$.

THE ISLANDED POWER PATH

Figure 9 assembles the elements into the islanded power path: charged power flows from the plasma through the DEC to a DC bus, which serves the base loads directly while the buffer store bridges the plasma lag and the black-start store cold-starts the plant. There is no rotating thermal machine in the primary electrical path, which is what permits the millisecond trim and the deep, grid-forming load-following demonstrated above.

Islanded power path of a fixed Aegis installation *(Schematic.)* Charged power is direct-converted ($\eta_{\mathrm{DEC}} = 0.49$) to a DC bus serving base loads; a 246 MWe / 1.1 MWh buffer bridges the plasma lag and an ≈ 18.4 MWh store provides black-start (AG-CX-20, AG-SX-01).

§ 5

Discussion

Against the tandem-mirror literature. The operating point sits within the physics envelope established by the classical tandem-mirror program [1,2] and revived by the simplified high-gain configuration of Fowler, Moir and Simonen [5,6]. The ambipolar-potential gate of equation (2), with $e\varphi_c/T_e \approx 2.77$ at $n_{\text{plug}}/n_{\text{cell}} = 16$, is squarely in the Pastukhov–Cohen regime [3,4]; the required plug over-density is specified by the frozen design, not assumed. The HTS axisymmetric-mirror results of WHAM [8] and the sustained hot-electron confinement of the gas-dynamic trap [9] are the contemporary experimental context that makes a high-field plugged mirror credible. Our contribution is not a new confinement claim but the coupling of this operating point to a quantified islanded electrical and fuel-cycle envelope.

Against the direct-conversion literature. The $\eta_{\text{DEC}} = 0.49$ composite efficiency on the 14.7 MeV proton channel is consistent with the venetian-blind and multi-grid electrostatic converters analysed since Moir and Barr [7]; the collector and architecture trades that support it are treated in companion papers. The operationally decisive point for islanded service is not the peak efficiency but the *absence of a thermal time constant*: because equation (6) is realised electrostatically, the trim of equation (8) is available at power-electronics speed, which is what enables the deep load-following of figure 2.

Against the microgrid literature. The islanded case is posed exactly as a grid-forming microgrid problem [12,13,14]: a dispatchable source, an energy buffer sized to the source's slowest actuator, and a black-start store. The buffer of equation (9), at 1.1 MWh and 246 MWe, is small precisely because the DEC is fast and only the ~ 8 s plasma lag must be bridged; this is a far lighter storage requirement than a thermal plant of comparable rating would impose [15]. Posing the throttle bound as a control-barrier constraint [16] inside a reference-governor law [17] places the load-following inside a certified safe set, in the same spirit as learned tokamak control [18] but with an explicit forward-invariance guarantee.

Against the helium-3 literature. The strategic reading of the fuel cycle follows Wittenberg–Santarius–Kulcinski [10,11]: terrestrial helium-3 is scarce (1–2 kg yr^{-1} domestic flow), the breeder's banked tritium-derived helium-3 (≈ 0.9 kg yr^{-1} per unit) is a strategic co-product rather than a closure mechanism, and fleet-scale demand (170.2 kg fpy^{-1} per burner) is met from lunar supply on a late-2030s schedule. The fleet-closure arithmetic of equation (15) makes the gap explicit: ~ 45–190 breeders per burner is not a deployable indigenous ratio, so the lunar gate is a genuine programmatic dependency, not a rhetorical one.

Companion results. This paper sits in the Kronos 2026 series. The burner physics core and its Q_E-closure gate are established in the Aegis forward-base burner paper [doi:10.5281/zenodo.22645693; https://www.kronosfusionenergy.com/publications/aegis-burner.html] and the recirculation-resolved closure [doi:10.5281/zenodo.22645860; https://www.kronosfusionenergy.com/publications/recirculation-resolved-q-e-closure-in-a-d-he-tandem-mir.html]; the direct-conversion basis in [doi:10.5281/zenodo.22645700; https://www.kronosfusionenergy.com/publications/direct-energy-conversion.html]; the neutron-lean siting case in [doi:10.5281/zenodo.22645917; https://www.kronosfusionenergy.com/publications/the-neutron-lean-siting-case-for-a-d-he-tandem-mirror-b.html]; the millisecond HVDC-native load interface in [doi:10.5281/zenodo.22645783; https://www.kronosfusionenergy.com/publications/metrovolt-hvdc-native-power-interface.html]; the non-closing helium-3 fuel cycle and lunar gate in [doi:10.5281/zenodo.22645734; https://www.kronosfusionenergy.com/publications/helium-3-fuel-cycle.html]; and the fleet tritium-breeding lever in [doi:10.5281/zenodo.22645706; https://www.kronosfusionenergy.com/publications/blanket-tritium-breeding-lever.html]. The present paper adds the islanded operating envelope and the fuel-cycle symbiosis that tie those results into a grid-independent installation.

§ 6

Limitations

The one honest gate is fleet-scale helium-3 supply. Equations (14)–(15) show that the indigenous breeder–burner flows seed and partly sustain the loop but do not close a plant-scale burner's $170.2\,\mathrm{kg\,fpy^{-1}}$ net demand at any deployable breeder-to-burner ratio; closure requires the lunar helium-3 supply on a late-2030s schedule. Near-term units run on bankable tritium-derived and self-bred helium-3, and the burn-lean mode and the light autonomy package stand independently of the lunar schedule, but the utility-scale fleet case rests on that gated input. Separately, the islanded load-following envelope of figure 2 is a modelled result built from the frozen envelope parameters (AG-CX-20, concept-class); the DEC-trim, buffer-rating and black-start numbers are adjudicated gates, while the full closed-loop demonstration on the plant twin is the next verification step.

§ 7

Conclusion

Aegis operates as a grid-independent fixed installation, and the case is quantitative rather than aspirational. At the frozen operating point ($Q_E = 1.318$, $f_n = 5.44\,\%$, $\eta_{\mathrm{DEC}} = 0.49$) the net electric output is near-linear in central-cell length — $+104.2/+850.0/+2831.9$ MWe at $55/440/1400$ m — at a first-wall load of 1.17 MW m^{-2}. Grid-independence closes end to end: a 0–104 MWe millisecond-class islanded load-following depth inside a certified stability bound, a 246 MWe / 1.1 MWh buffer that bridges the 8 s plasma lag, an ≈ 18.4 MWh black-start store, and a ~ 1 t one-year fuel package whose binding quantity is a 0.5 kg day^{-1} makeup throughput. The fuel closes a breeder–burner helium-3 symbiosis — breeder-banked tritium decaying to helium-3 (≈ 0.9 kg yr^{-1} per unit), $\approx 18\,\%$ in-machine recycle, and ≈ 32 kg fpy^{-1} of self-bred tritium — seeded indigenously and scaled from lunar supply, and a burn-lean mode removes $60\,\%$ of the neutron power for $\approx 4\,\%$ of fusion power, giving a tunable neutron signature. These properties follow directly from the aneutronic, direct-conversion, linear-mirror architecture, and together they constitute a defensible, auditable basis for grid-independent fusion power at a defense installation.

Acknowledgments tocsectionAcknowledgments Part of the Kronos Fusion Energy 2026 design series. Kronos Fusion Energy is a family-owned American company. The authors thank the Kronos physics de-risking programme for the frozen result set underlying every quantitative claim. Computation was performed on the NVIDIA GPU HPC campaign.

Reproducibility. The islanded-operation, black-start, fuel-autonomy and helium-3-flow results are frozen gates in the Kronos Physics De-Risking Register (KX-L1-A9, AG-CX-20, AG-SX-01, AG-L1-A8, AG-CX-17, AG-L1-A6, BR-OUT-2, BR-CX-16, MV-CX-29, AG-CX-14, AG-CX-16, BR-OUT-4) and are regenerable from the frozen 0-D mirror power-balance solver, the Kronos toolkit fuel-cycle model, the Monte-Carlo neutronics and the microgrid dispatch simulator, together with the figure-generation script deposited with this paper. This paper is archived at doi:10.5281/zenodo.22645862 and its official version is at https://www.kronosfusionenergy.com/publications/islanded-forward-base-operation-of-the-aegis-d-he-tande.html; the register is at doi:10.5281/zenodo.22133057.

Data availability tocsectionData availability This paper is archived at doi:10.5281/zenodo.22645862. The islanded-envelope, black-start, fuel-autonomy and helium-3-flow inputs used for figures 1–9 are archived with the deposit and reference the Kronos 2026 series; all quantitative values trace to the register (doi:10.5281/zenodo.22133057) by the serial identifiers cited inline. Any economic analysis is reported separately and is not part of the public deposit.

Competing interests tocsectionCompeting interests Provisional patent applications relating to aspects of this work have been filed.

tocsectionReferences

APPARATUS

Portfolio, People & Record

The intellectual-property estate, the people who built it, the limitations that gate it, and the sources it rests on.

1	4	40	27
GRANTED PATENT	2026 PROVISIONALS	TEAM MEMBERS	2022 PROVISIONALS

INTELLECTUAL PROPERTY

The patent portfolio

The estate spans a granted high-field magnet patent, pending utility and 2026 provisional filings that map to the two products, a digital-twin control provisional, a registered trademark application, and the original 2022 provisional family. Every patentable disclosure in the five-paper arXiv drop was protected **before** publication: the breeder and burner provisionals were filed 1–2 August, and a publication-gap omnibus filing the evening before the drop swept up the DEC, plasma-control, and REBCO-winding matter of the three otherwise-unprotected papers. Patent numbers and application serials are matters of public record; claim scope is summarised, not reproduced.

GRANTED & PENDING UTILITY

US 12,009,112	High-field tilted graded-REBCO magnet architecture (KRONO-002A) · *app. 17/878,550*	GRANTED
US 17/878,507	Core device / method (KRONO-001A) · *utility*	PENDING

2026 PROVISIONAL FILINGS — MAPPED TO THE PRODUCTS

64/124,209	Hyperion — spherical-tokamak tritium / helium-3 foundry · *breeder · filed Aug 2026*	FILED
64/124,220	Aegis / MetroVolt — synchrotron-cutoff, fuel-selection & plug-winding · *generator · filed Aug 2026*	FILED
64/115,167	KRONOS-CTRL digital-twin plant control · *provisional · filed Jul 2026*	FILED
64/005,440	Integrated spherical-tokamak fusion architecture · *early integrated-architecture filing · filed Mar 2026*	FILED
64/105,530	Negative-triangularity spherical-tokamak architecture · *foundational ST filing · filed Jul 2026*	FILED
64/128,097	Publication-gap omnibus — quasineutral two-species expander DEC · provenance-gated / latency-split plasma control · as-built high-field winding & conductor architecture · *filed 7 Aug 2026, the evening before the arXiv drop*	FILED

TRADEMARK & ORIGIN

FTK-98801894	Kronos Fusion Energy — trademark application	FILED
KR-2022-*	Original provisional family (KR-2022-00001 … 00027) · *27 filings, 2022*	PRIORITY

The narrow, defensible magnet novelty — the specific conductor and the digital-twin winding optimisation, not high-field REBCO as a category — is the commercial core that can earn ahead of any Q > 1 milestone, with markets in fusion magnet supply, MRI/NMR, accelerators, and proton therapy. The claim is scoped honestly: the high field is a *system field* result, not a stand-alone-coil record; the small-bore plug coil is structurally infeasible as a bare winding but resolved by a stress-managed structural shield (feasible-pending-FEA); and the winding-tape experiment returned a *null result*. The value is the method, not a field record.

THE TEAM

Founding partners, board, advisors & auditors

Kronos is built by a bench of advanced-fuel-fusion, high-field-magnet, direct-conversion, and materials specialists, with a board and operations team drawn from defense, national laboratories, and industry. Dates are shown as ranges; where a tenure has ended or is term-ending, the range says so.

FOUNDING PARTNERS — SCIENCE

Dr. Gerald Kulcinski
Co-Founder · Helium-3 & Advanced-Fuel Fusion
UW–Madison · 2023–Present

Dr. Carl Weggel
Chief Scientist / S.M.A.R.T. Design
MIT Alcator Program · 2022–Present

Dr. Robert J. Weggel
Magnetic Field Design
MIT Magnet Lab · 2022–Present

BOARD

Priyanca Ford
Founder & CEO · Executive Board
2022–Present

Bandel Carano
Finance / Strategy
Oak Investment Partners / Stanford · 2025–2026

Patrick Schweiger
Fusion Device Engineering
Oklo / CFS / TerraPower · 2025–Present

SCIENTIFIC ADVISORS

Dr. Steven O. Dean
Fusion Policy & History
DOE / Fusion Power Associates · 2025–Present

Dr. Patrick H. Diamond
Plasma Turbulence & Transport
UC San Diego · 2025–Present

Dr. Jack J. Dongarra
HPC & Numerical Algorithms
Turing Award · 2025–Present

Dr. Nasr M. Ghoniem
Chief Material Scientist
UCLA · 2025–Present

Dr. Siegfried Glenzer
Plasma Physics & Laser Fusion
Stanford / SLAC · 2022–Present

Dr. David A. Hammer
Pulsed-Power Fusion
Cornell · 2025–Present

Dr. Donald A. Spong
Plasma Theory & Confinement
ORNL · 2025–Present

Dr. Curtis Smith
Risk Assessment & Nuclear PRA
MIT / Idaho National Lab · 2025–Present

RADM (Ret.) David Goggins
Naval Engineering & Power-Plant Design
U.S. Navy · 2023–2026

Dr. Konstantin Batygin
Mathematician
Caltech · 2022–2025

Dr. Ruben Fair
Magnet Design / ITER Liaison
PPPL / Jefferson Lab · 2022–2025

Dr. Paul S. Weiss
Materials & Nanotechnology
UCLA · 2022–2025

SCIENTIFIC AUDITORS

Dr. Wilfred A. Cooper
Plasma Equilibrium Theory
EPFL / Swiss Plasma Center · 2025–Present

Dr. Ahmed Hassanein
Plasma–Material Interactions
Purdue / Argonne · 2025–Present

Dr. Patrick E. Hopkins
Extreme Thermal Materials
U. of Virginia · 2025–Present

Dr. Peter Hosemann
Materials Joining & Structural Integrity
UC Berkeley · 2025–Present

Dr. Travis W. Knight
Advanced Nuclear Fuels & Systems
U. of South Carolina · 2025–Present

Dr. Philippe Lebrun
Cryogenics & Magnet Cooling
CERN · 2025–Present

Dr. Nitendra Singh
Nuclear Safety & Fuel Cycle
ITER · 2025–Present

Dr. Guido Van Oost
Magnetic Confinement & Fusion Systems
Ghent University · 2025–Present

Dr. Gary S. Was
Radiation Materials & Structural Integrity
U. of Michigan · 2025–Present

Dr. Ray Sedwick
Direct Energy Conversion
U. of Maryland · 2025

OPERATIONS

Michael Laughlin
Chief Operating Officer
2022–Present

Martin Owens
Chief Strategy Officer
LANL / GE Hitachi · 2022–Present

MG (Ret.) Paul Pardew
Chief Contracting Officer
Army Contracting Command · 2022–Present

David Beck
Fusion Commercialization
U.S. Space Force · 2024–Present

Sushma Bhatia
Environmental & Legislative
Google · 2022–Present

Michael De Frenza
Technology Licensing
2023–Present

MG (Ret.) Robin L. Fontes
Cybersecurity & Defense
Army Cyber Command · 2022–Present

Vijay Gehani
Supply Chain & Components
INOX India · 2024–Present

Jon Michel Greenwood
IT & AI Infrastructure
Live Nation · 2023–Present

Brian C. O'Neill
National Security
CIA / ODNI · 2022–Present

Gen. (Ret.) Gustave F. Perna
DoD Liaison
Operation Warp Speed · 2022–2023

Andrea Romero
Marketing Lead
2022–Present

Legal counsel is retained; those roles are held on the internal roster and are not listed here.

SOURCES

References

1 D E Baldwin and B G Logan, Improved tandem mirror fusion reactor, *Phys. Rev. Lett.* **43** 1318 (1979). doi:10.1103/PhysRevLett.43.1318

2 R F Post, The magnetic mirror approach to fusion, *Nucl. Fusion* **27** 1579 (1987). doi:10.1088/0029-5515/27/10/001

3 V P Pastukhov, Collisional losses of electrons from an adiabatic trap in a plasma with a positive potential, *Nucl. Fusion* **14** 3 (1974). doi:10.1088/0029-5515/14/1/001

4 R H Cohen, M E Rensink, T A Cutler and A A Mirin, Collisional loss of electrostatically confined species in a magnetic mirror, *Nucl. Fusion* **18** 1229 (1978). doi:10.1088/0029-5515/18/9/005

5 T K Fowler, R W Moir and T C Simonen, A new simpler way to obtain high fusion power gain in tandem mirrors, *Nucl. Fusion* **57** 056014 (2017). doi:10.1088/1741-4326/aa5e54

6 T C Simonen, Three game changing discoveries: a simpler fusion concept?, *J. Fusion Energy* **35** 63 (2015). doi:10.1007/s10894-015-0017-2

7 R W Moir and W L Barr, "Venetian-blind" direct energy converter for fusion reactors, *Nucl. Fusion* **13** 35 (1973). doi:10.1088/0029-5515/13/1/005

8 D Endrizzi *et al*, Physics basis for the Wisconsin HTS Axisymmetric Mirror (WHAM), *J. Plasma Phys.* **89** 975890501 (2023). doi:10.1017/S0022377823000806

9 P A Bagryansky *et al*, Threefold increase of the bulk electron temperature of plasma discharges in a magnetic mirror device, *Phys. Rev. Lett.* **114** 205001 (2015). doi:10.1103/PhysRevLett.114.205001

10 L J Wittenberg, J F Santarius and G L Kulcinski, Lunar source of ^{3}He for commercial fusion power, *Fusion Technol.* **10** 167 (1986). doi:10.13182/FST86-A24972

11 L J Wittenberg, E N Cameron, G L Kulcinski *et al*, A review of ^{3}He resources and acquisition for use as fusion fuel, *Fusion Technol.* **21** 2230 (1992).

12 N Hatziargyriou, H Asano, R Iravani and C Marnay, Microgrids, *IEEE Power Energy Mag.* **5**(4) 78 (2007). doi:10.1109/MPAE.2007.376583

13 F Katiraei, R Iravani, N Hatziargyriou and A Dimeas, Microgrids management, *IEEE Power Energy Mag.* **6**(3) 54 (2008). doi:10.1109/MPE.2008.918702

14 R H Lasseter, Z Chen and D Pattabiraman, Grid-forming inverters: a critical asset for the power grid, *IEEE J. Emerg. Sel. Topics Power Electron.* **8** 925 (2020). doi:10.1109/JESTPE.2019.2959271

15 K C Divya and J stergaard, Battery energy storage technology for power systems — an overview, *Electr. Power Syst. Res.* **79** 511 (2009). doi:10.1016/j.epsr.2008.09.017

16 A D Ames, X Xu, J W Grizzle and P Tabuada, Control barrier function based quadratic programs for safety critical systems, *IEEE Trans. Autom. Control* **62** 3861 (2017). doi:10.1109/TAC.2016.2638961

17 D Q Mayne, J B Rawlings, C V Rao and P O M Scokaert, Constrained model predictive control: stability and optimality, *Automatica* **36** 789 (2000). doi:10.1016/S0005-1098(99)00214-9

18 J Degrave *et al*, Magnetic control of tokamak plasmas through deep reinforcement learning, *Nature* **602** 414 (2022). doi:10.1038/s41586-021-04301-9

19 P K Romano, N E Horelik, B R Herman, A G Nelson, B Forget and K Smith, OpenMC: a state-of-the-art Monte Carlo code for research and development, *Ann. Nucl. Energy* **82** 90 (2015). doi:10.1016/j.anucene.2014.07.048

20 R Delaporte-Mathurin *et al*, Finite element analysis of hydrogen retention in ITER plasma facing components using FESTIM, *Nucl. Mater. Energy* **21** 100709 (2019). doi:10.1016/j.nme.2019.100709

21 J E Menard *et al*, Fusion nuclear science facilities and pilot plants based on the spherical tokamak, *Nucl. Fusion* **56** 106023 (2016). doi:10.1088/0029-5515/56/10/106023

COLOPHON

How this document was made

The Kronos Fleet — Combined Editorial, 2026 is set in **Fraunces** (display), **Gelasio** (text), and **IBM Plex Mono** (data & equations), carried forward from the Kronos editorial design system.

The figures are rendered at 300 dpi from the deposited generator scripts; the document is composed as a single self-contained file with embedded fonts and imagery, paginated to US Letter, and rendered to PDF through a headless Chromium engine in matched light and dark editions.

Every headline quantity carries an evidence class; withdrawn and restated values are marked as such. Nothing herein is frozen beyond the founder-approved Tier-A set.

Explore it live — turn the interactive 3-D model, run the deposited solvers in the physics validator, and watch the companion film series.

LEGAL NOTICE

Notice, status, and distribution

Conceptual design & simulation study. This document reports a conceptual design and simulation study. It is not a construction commitment, a safety-analysis report, a regulatory filing, or an offer of securities. Forward-looking statements — schedules, costs, market sizes, and performance — are estimates subject to the limitations set out in the Simulations part and may change.

Numbers and their classes. Quantities are reported with evidence classes and case labels; modelled, assumed, and requirement-class values are identified as such and are not to be quoted without their labels.

Public edition. This edition carries the physics and design only; all financial, funding, and defense-commercial content has been removed for public distribution. The scientific text corresponds to the arXiv and journal submissions.

THE 2026 KRONOS SERIES

One programme, many papers

This editorial is one paper in the Kronos 2026 series — a real fusion company's complete, reproducible physics record for a spherical-tokamak breeder and its low-neutron D–^{3}He tandem-mirror burners. Every headline number is a frozen anchor in the Physics De-Risking Register.

Explore the whole programme: the De-Risking Register, the interactive 3-D model, and the physics validator.

KRONOS FUSION ENERGY

Islanded Forward-Base Operation of the Aegis D-^{3}He Tandem-Mirror Burner: Black-Start, Microgrid Load-Following, and the Lunar-Gated He-3 Symbiosis

A real fusion company building real machines. Explore the science, live.

Zenodo · doi:10.5281/zenodo.22645862

Read on kronosfusionenergy.com

The Physics De-Risking Register